Accelerating the acquisition of high-resolution quadrupolar MQ/ST-HETCOR 2D spectra under fast MAS via 1H detection and through-space population transfers.

A. Sasaki, Julien Trebosc, Jean-Paul Amoureux

ARTICLE

Accelerating the acquisition of high-resolution quadrupolar MQ/ST-HETCOR 2D spectra under fast MAS via ^{1}H detection and through-space population transfers

Received 00th January 20xx,
Accepted 00th January 20xx

DOI: 10.1039/x0xx00000x

Akiko Sasaki,[a] Julien Trébosc,[b] Jean-Paul Amoureux*[b,c,d]

Recently, we established an experimental setup protocol to perform the population transfer from half-integer quadrupolar spin to ^{1}H nuclei under fast MAS in the context of MQ-HETCOR experiments. In this article, we further develop the high-resolution 2D HETCOR methods by ST-based approaches, making use of the sensitivity advantage of STMAS over its MQMAS counterpart. In a similar manner to the previous work, which utilized CP and RINEPT for the population transfer, we also demonstrate the experimental setup protocol for PRESTO. Using {^{23}Na}-^{1}H and {^{27}Al}-^{1}H spin systems of powder samples, we compare a series of MQ/ST-HETCOR 2D spectra to discuss the pros and cons of the distinct MQ/ST-based approaches for spin 3/2 and 5/2 nuclei, respectively. We also incorporate two experimental tricks to reduce the experimental time of such long 2D experiments, the Optimized Rotor-Synchronization (ORS) and the Non-Uniform Sampling (NUS), in the context of high-resolution spectra of half-integer quadrupolar spin nuclei.

I. Introduction

In solid-state NMR, owing to the technical development of fast magic angle spinning (MAS) probes and small-diameter rotors, higher spinning rates have become more and more accessible on an everyday basis. The higher ^{1}H resolution under fast MAS conditions is particularly advantageous for ^{1}H-detected two-dimensional (2D) HETCOR (HETero-nuclear CORrelation) experiments.[1–10]

Quadrupolar nuclei, with spin I > ½, are subject to the quadrupole interaction, which results from the coupling between the electric quadrupole moment of the nucleus and the electric field gradients at the nucleus. This quadrupole interaction can be described as an expansion with respect to the Zeeman interaction: $H_Q = H_{Q1} + H_{Q2} + \ldots$. In the case of half-integer quadrupolar nuclei (I = 3/2, 5/2, 7/2 and 9/2), two types of resonances are observed: the central transition (CT: +1/2 ↔ -1/2) and the satellite transitions (ST: m ↔ m-1 with m ≠ ½). All resonances are subject to an anisotropic quadrupolar broadening. Therefore, high-resolution 2D methods, such as multiple-quantum MAS (MQMAS)[11] and satellite-transition MAS (STMAS)[12] experiments, are required to obtain isotropic spectra in the indirect dimension. This is also the case of high-resolution HETCOR spectra involving half-integer quadrupolar spin nuclei.

A high-resolution HETCOR experiment can start from the spin-1/2 nucleus, but it then requires a 3D time-consuming acquisition.[13] Therefore, to only use a 2D scheme and to profit of the often short relaxation time of the quadrupolar spin nuclei, high-resolution HETCOR experiments often start from the quadrupolar spin nucleus through an MQMAS or STMAS quadrupolar filter and end in the detection of the spin-1/2 nucleus. The population transfer from the quadrupolar to the spin-1/2 nuclei can be done either with CP (MQ-CP-HETCOR[1,14–19] and ST-CP-HETCOR[20]), or RINEPT (MQ-J-RINEPT[19,21–24] or MQ-D-RINEPT[2,3,22,25]). The vast majority of these high-resolution HETCOR experiments with a transfer from a half-integer spin quadrupolar to a spin-1/2 nucleus has been performed with {^{27}Al}-^{31}P, {^{27}Al}-^{27}Si and {^{23}Na}-^{31}P under slow MAS conditions. Other variants of the 2D HETCOR sequences include two consecutive population transfers, such as the MQ-J-HMQC[13] and HMQC-ST[4] approaches.

Very recently, we have utilized the sensitivity advantage of the high-resolution ^{1}H detection under fast MAS in dipolar-mediated MQ-HETCOR experiments, using two spin-systems: {^{23}Na}-^{1}H and {^{27}Al}-^{1}H.[26] We demonstrated the experimental setup protocol for CP and RINEPT transfers to acquire MQ-HETCOR 2D spectra with the best possible quality for a given amount of spectrometer time. We have also shown that the use of the SPAM (Soft-Pulse Added-Mixing) sensitivity gain[27–31] is beneficial for MQ-HETCOR experiments as the MQ excitation/conversion efficiency decreases with increasing MAS frequency.[32]

[a] Bruker Japan K.K., 3-9, Moriya-cho, Kanagawa-ku, Yokohama-shi, Kanagawa 221-0022, Japan.
[b] Univ. Lille, CNRS, Centrale Lille, ENSCL, Univ. Artois, UMR 8181 – UCCS – Unit of Catalysis and Chemistry of Solids, F-59000 Lille, France.
[c] Bruker Biospin, 34 rue de l'industrie, F-67166 Wissembourg, France.
[d] RIKEN RSC NMR Science and Development Division, 1-7-22 Suehiro-cho, Tsurumi-ku, Yokohama-shi, Kanagawa, 230-0045, Japan.

Electronic Supplementary Information (ESI) available. See DOI: 10.1039/x0xx00000x

In this article, we further develop the high-resolution 2D HETCOR methods in the context of ST-based experiments, making use of the sensitivity advantage of STMAS over MQMAS. In a similar manner to the previous work, which utilized CP and RINEPT for the population transfer, we demonstrate the experimental setup protocol for PRESTO approaches, and we also exploit the SPAM sensitivity advantage upon acquisition of MQ/ST-HETCOR spectra. We perform a comparison of the {^{23}Na}-^{1}H and {^{27}Al}-^{1}H MQ/ST-HETCOR 2D spectra to discuss the pros and cons of the MQ/ST-based approaches for I = 3/2 (^{32}Na) and 5/2 (^{27}Al) nuclei, using a variety of crystalline test samples. Furthermore, we also incorporate two experimental tricks to reduce the experimental time of such long 2D experiments: the optimized rotor-synchronization (ORS) and the non-uniform sampling (NUS). Both tricks are applicable not only to MQ/ST-HETCOR, but also to MQ/STMAS experiments. We experimentally demonstrate the practical advantage of the ORS and discuss the potential use of NUS in the context of high-resolution spectra of half-integer quadrupolar spin nuclei.

In Figs.1 and 2, we summarize the pulse sequences and coherence transfer pathways used in this study, for {^{27}Al}-^{1}H and {^{23}Na}-^{1}H transfers, to show the distinct approaches used for I larger or equal to 3/2, respectively. We note that MQ-HETCOR experiments are similar between I = 3/2 and 5/2, as only the R_{MQ} coefficients and the coherence transfer pathways (i.e. the phase cycling) differ. On the contrary, for the ST-HETCOR approaches, either the STMAS filter is used for I ≥ 5/2, while it is the DQ-STMAS version for I = 3/2 due to the practicality of the desired coherence selection.

Compared to the previous studies, we have shortened the minimum total number of phases of the MQ/ST-HETCOR

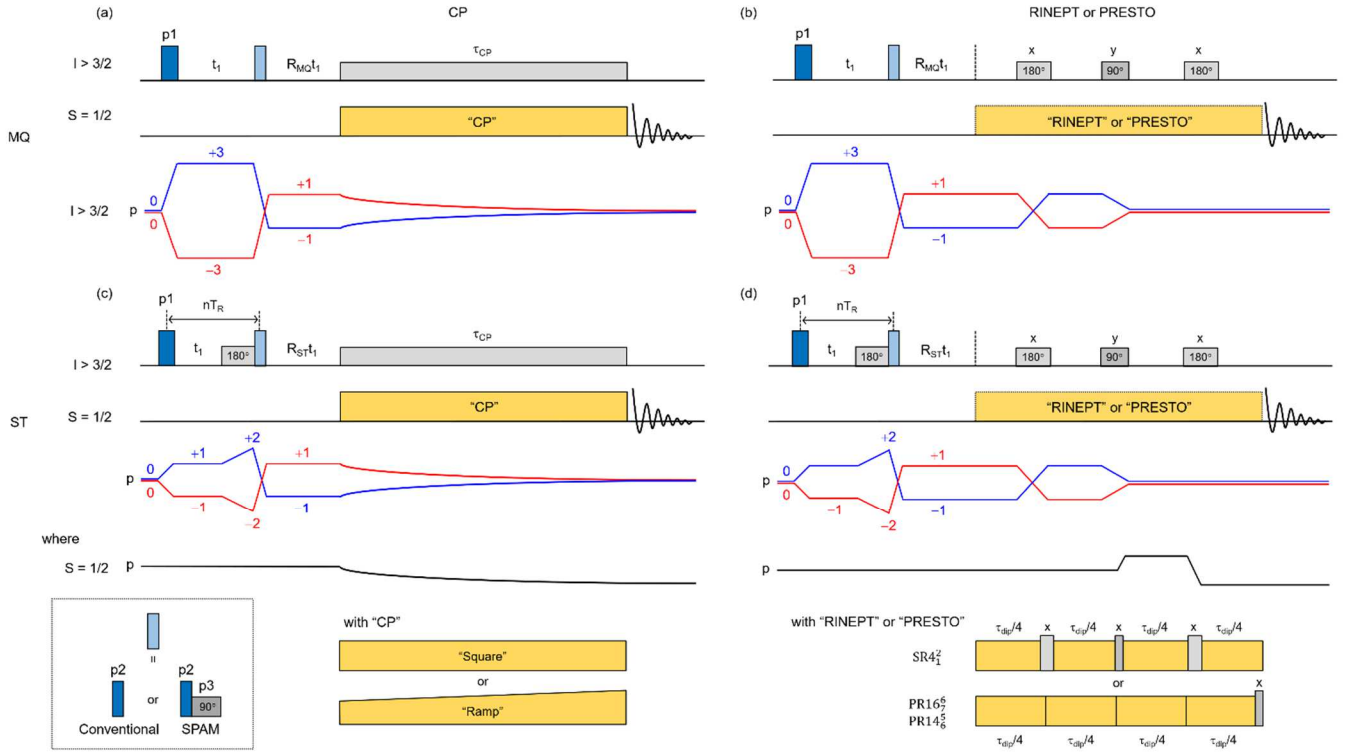

Fig.1. [IN COLOR] Pulse sequences and coherence transfer pathways used in the following for {I > 3/2}-^{1}H (a,b) MQ-HETCOR and (c,d) ST-HETCOR experiments via population transfer by (a,c) CP and (b,d) RINEPT or PRESTO. {R_{MQ} , R_{ST}} = {38, 7}/24, {101, 28}/45 and {182, 55}/72 for the innermost ST of I = 5/2, 7/2 and 9/2, respectively. In (b,d), the three quadrupolar pulses in RINEPT and PRESTO are CT-selective.

sequences to $N_{\varphi,tot}$ {MQ, ST} = {24, 24} (I > 3/2) and {24, 16} (I = 3/2). This shortening allows accelerating the signal acquisition and hence facilitates the experimental optimization. The SPAM signal enhancement occurs when transferring from 3Q to 1Q levels, not to 0Q. Therefore, the SPAM enhancement, shown with the composite pale blue pulse in Figs.1,2, is used for I = 3/2 MQ-HETCOR and I = 5/2 MQ/ST-HETCOR. It cannot be employed with DQ-ST-HETCOR experiments (I = 3/2).

In this work, the population transfers from the quadrupolar to ^{1}H nucleus are performed by either the ramp-CP, RINEPT or PRESTO schemes.

II. Methods

All experiments were performed using a Bruker Avance NEO spectrometer with a B_0 = 14.1 T wide-bore magnet with Larmor frequencies of 158.8 (^{23}Na), 156.5 (^{27}Al) and 600.3 (^{1}H) MHz, equipped with a 1.3 mm HX MAS probe. A maximum rf field strength of $\nu_1 \approx 150$ kHz was attainable with this probe for ^{23}Na, ^{27}Al and ^{1}H. We have used five powder test samples: NaH_2PO_4, Na_2HPO_4, sodium citrate dihydrate (NaCD), ipa-AlPO-14 and a 1:1 molar mixture of aluminum acetylacetonate and lactate (Al-acet-lact). These samples were packed as purchased or as synthesized. The chemical shifts of the samples were used as secondary references. The ^{23}Na or ^{27}Al indirect

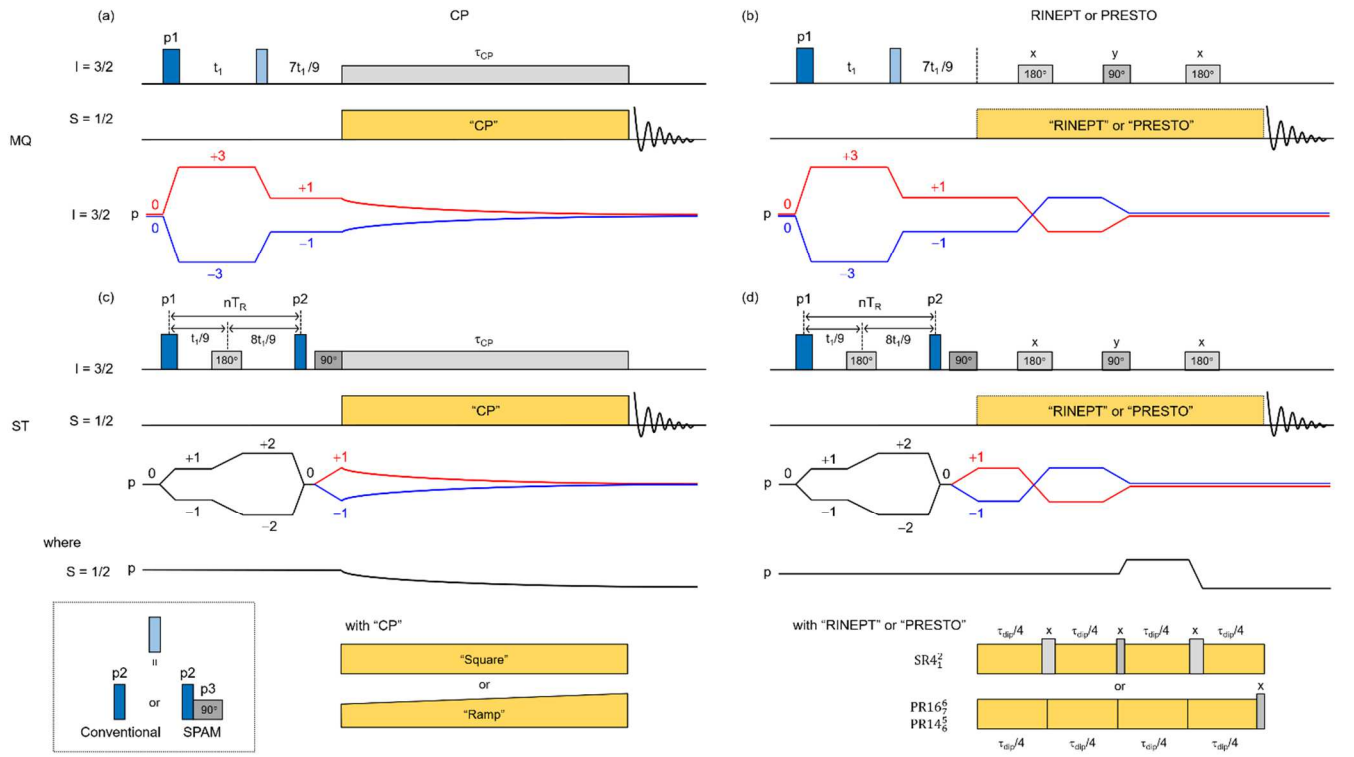

Fig.2. [IN COLOR] Pulse sequences and coherence transfer pathways used in the following for {I = 3/2}-^{1}H (a,b) MQ-HETCOR and (c,d) ST-HETCOR experiments via population transfer by (a,c) CP and (b,d) RINEPT or PRESTO. In (b,d), the three quadrupolar pulses in RINEPT and PRESTO are CT-selective.

isotropic dimensions of the 2D HETCOR spectra were referenced according to the unified representation.[33] The 4.0.6 version of the Topspin software was used throughout. We provide in the SI our TopSpin pulse sequences for ST-HETCOR experiments, those for MQ-HETCOR being in the SI of our previous article.[26]

As in STMAS, ST-HETCOR requires refocusing of the first-order quadrupole interaction of the satellite transitions, and hence the accurate magic angle setting (e.g. 54.736 ± 0.002°) and the stable spinning stability (e.g. 1 part in 10^4) are a prerequisite to acquire perfect 2D spectra.[33–35] In this study, the magic angle was set on the sample of interest itself, using the split-t_1 DQF-STMAS pulse sequence,[36] prior to the acquisition of ST-HETCOR spectra. The spinning stability was maintained by a MAS III unit within ±10 Hz at ν_R = 20 or 62.5 kHz.

All MQ/STMAS simulations were performed using the SIMPSON simulation programs.[37] The input parameters were the nucleus of interest (^{23}Na or ^{27}Al), the spinning frequency (ν_R), the rf-field strength (ν_1) and the quadrupolar coupling constant (C_Q). The quadrupole interaction, with η_Q = 0, was taken into account up to the second-order, without scalar or dipolar coupling. The powder averaging parameters (crystal file and number of γ-angles) and the Δt maximum time step (over which the Hamiltonian is considered time independent) were tested for convergence, and a combination of ZCW20 × 10 γ-angles with Δt = 0.1 μs was sufficient for the given range of C_Q values used in the plot. Since the imaginary part of the signal was found to be minor, only the real part is plotted as the signal intensity.

III. Setting up the experiments

It should be particularly emphasized that we make use of the ^{1}H resolution advantage under fast MAS to perform ^{1}H-detected high-resolution quadrupolar HETCOR experiments. In the 2D HETCOR spectra, the ^{1}H MAS spectrum is in the direct dimension and the isotropic ^{23}Na or ^{27}Al spectrum is in the indirect one. In our previous study,[26] we have shown a series of ^{23}Na, ^{27}Al and ^{1}H 1D MAS spectra at ν_R = 20 and 62.5 kHz for NaH_2PO_4, Na_2HPO_4, NaCD and ipa-AlPO-14 to demonstrate the advantage of ^{1}H detection under fast MAS. We additionally show, in Fig.**3**, the equivalent set of ^{27}Al and ^{1}H MAS 1D spectra of Al-acet-lact. For the second-order broadened ^{27}Al quadrupolar frequencies, there is no obvious change between the two MAS rates, except for the presence/absence of small spinning sidebands, whereas the ^{1}H MAS spectrum changes in both intensity and appearance at the two spinning rates. In this case of our 'artificial' mixture of two Al powder samples, we note the presence of two C-H signals, at 4 and 5 ppm, which are resolved at ν_R = 62.5 kHz, each originating from one of the two samples. We demonstrate in this work that these two resonances can be unambiguously assigned upon correlation with Al species. Overall, the higher resolution under fast MAS has a greater potential to provide structural information that could not be detected under slow MAS in

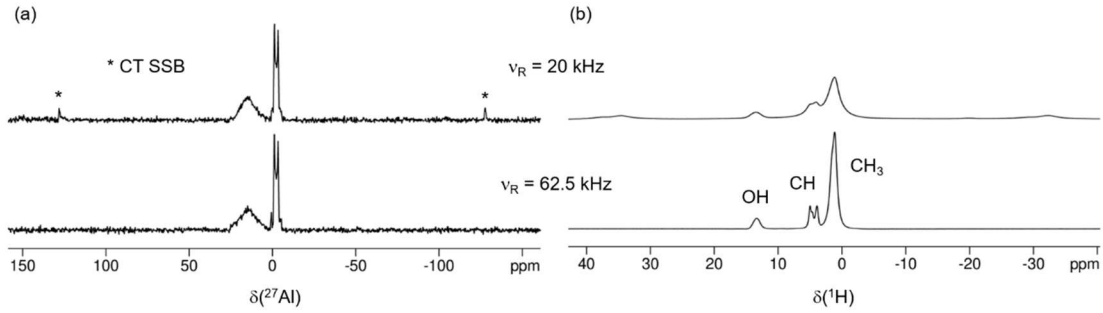

Fig.3. Examples of (a) ^{27}Al and (b) ^{1}H MAS 1D spectra at ν_R = 20 (top) and 62.5 kHz (bottom), using 1:1 molar mixture of aluminum acetylacetonate and aluminum lactate. (a) NS = 8, RD = 3 s, T_{exp} = 24 s each. (b) NS = 1, RD = 1 s, T_{exp} = 1 s each.

each of the five compounds used in the following HETCOR investigations.

In the following subsections, we briefly review and describe the experimental protocol of CPMAS, RINEPT, PRESTO and SPAM, based on practical considerations to set up ^{1}H-detected MQ/ST-HETCOR experiments under fast MAS.

III.1. Setting up CPMAS and RINEPT

The efficiency of the transfer from quadrupolar to ^{1}H nuclei inherently depends on several parameters such as: the rf-fields ($\nu_{1,H}$ for ^{1}H and $\nu_{1,I}$ for the quadrupolar spin nucleus), the spinning rate (ν_R), the offset, the quadrupole interaction described with $\nu_Q = 3C_Q/(2I(2I-1))$, and the magnitude of the ^{1}H-I dipolar interactions (b_{HI}). Since we have described in the previous work the detailed setup procedure for CPMAS and RINEPT, here we only provide the essence of the practical points to be reminded upon quadrupolar I $\rightarrow$ ^{1}H transfers under fast MAS (e.g. ν_R = 62.5 kHz).

CPMAS. (i) The most efficient way to perform a CPMAS transfer with a half-integer quadrupolar nucleus is to use the sudden-passage regime.[38] (ii) This condition requires a very low $\nu_{1,I}$ rf-field of a few kHz. (iii) The efficiency strongly depends on $\nu_{1,H}$ by as small as 5-10 kHz variations. (iv) The ramp shaped pulses, which will be used in the following, perform better than the conventional square pulses, as often observed with spin-1/2 systems. (v) For a given sample, optimizing the contact time (τ_{CP}) is a prerequisite, and for the sake of sensitivity, a long initial value, $\tau_{CP} \approx$ 3-4 ms, may be recommended in most cases. However, if one wishes to observe directly bonded species (such as ^{17}O-H), much shorter contact times would be more appropriate. (vi) For 'molecular' systems, e.g. NaCD and ipa-AlPO-14, the transfer efficiencies may decrease due to the presence of dynamics, necessitating the use of an increased number of scans (NS) to achieve an acceptable SNR.

RINEPT. (i) The dipolar recoupling is based on the γ non-encoded symmetry-based $SR4_1^2$ scheme. The refocusing block $R4_1^2 = 180_{90}180_{270}180_{90}180_{270}$, which lasts one rotor period (T_R) is super-cycled to $[R4^2_1R4^{-2}_1]_0[R4^2_1R4^{-2}_1]_{120}[R4^2_1R4^{-2}_1]_{240}$. (ii) When using a rectangular π-pulse as basic element, the ^{1}H irradiation is applied with $\nu_{1,H} = 2\nu_R$ = 125 kHz at ν_R = 62.5 kHz. (iii) Using a $\{270_0,90_{180}\}$ basic element is more efficient than a square pulse,[39] but it requires a too large rf-field for our probe: $\nu_{1,H} \approx 3.5\nu_R \approx$ 200 kHz at ν_R = 62.5 kHz. (iv) The three CT-selective pulses on the quadrupolar channel use a low rf-field of a few kHz. In this study, the durations of the $\pi/2$ and π-pulses have been fixed for RINEPT and PRESTO experiments at 8 ($T_R/2$) and 16 µs (T_R), for the $\pi/2$ and π-pulses, respectively. (v) The recoupling period may be predicted from the b_{HI} dipolar coupling constant (in rad/s) with the relation, $\tau_{dip} \approx 20/b_{HI}$ with {180} basic element,[40] and then optimized experimentally, especially for 'molecular' systems.

III.2. Setting up PRESTO

The PRESTO sequence[41] uses γ-encoded symmetry-based recoupling schemes, which will be labelled $\mathbf{PRN}_n^\nu$. The schematic illustration of the two efficient PRESTO sequences used in this work, $PR16_7^6$ and $PR14_6^5$, is shown in Fig.**4** using a composite $\{270_0, 90_{180}\}$ pulse as basic element. This sequence suppresses the ^{1}H isotropic chemical shifts, the hetero-nuclear J-couplings and the ^{1}H-^{1}H dipolar couplings to the first-order.[39]

With respect to the RINEPT scheme, the quadrupolar channel is identical with the same three CT-selective pulses, whereas for the ^{1}H channel, (i) there is no delay between the four blocks of PRESTO, and (ii) a $\pi/2$ read-out pulse is added at the end because PRESTO acts on the S_z magnetization.

As an example, Fig.**S1** presents the ^{23}Na $\rightarrow$ ^{1}H PRESTO transfer 1D profiles of NaH_2PO_4 with $PR16_7^6$ and $PR14_6^5$ recouplings at ν_R = 62.5 kHz, upon varying: the

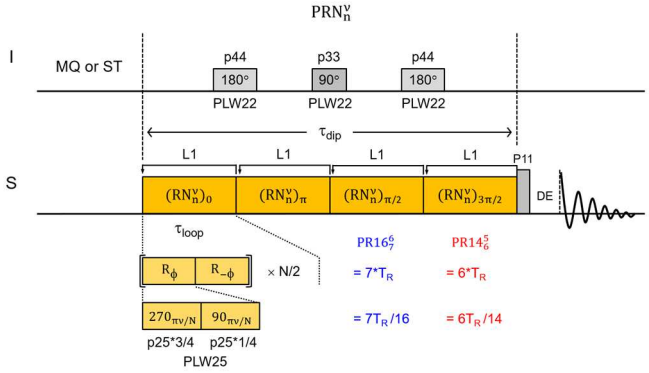

Fig.4. Schematic illustration of two PRESTO ($R16_7^6$ and $R14_6^5$) recoupling schemes used in this study. A $\pi/2$ read-out pulse (P11) is added at the end of the PRESTO blocks. At ν_R = 62.5 kHz, the theoretical optimum $\nu_{1,H}$ (PLW25) = 143 ($16\nu_R/7$) and 146 kHz ($14\nu_R/6$), respectively.

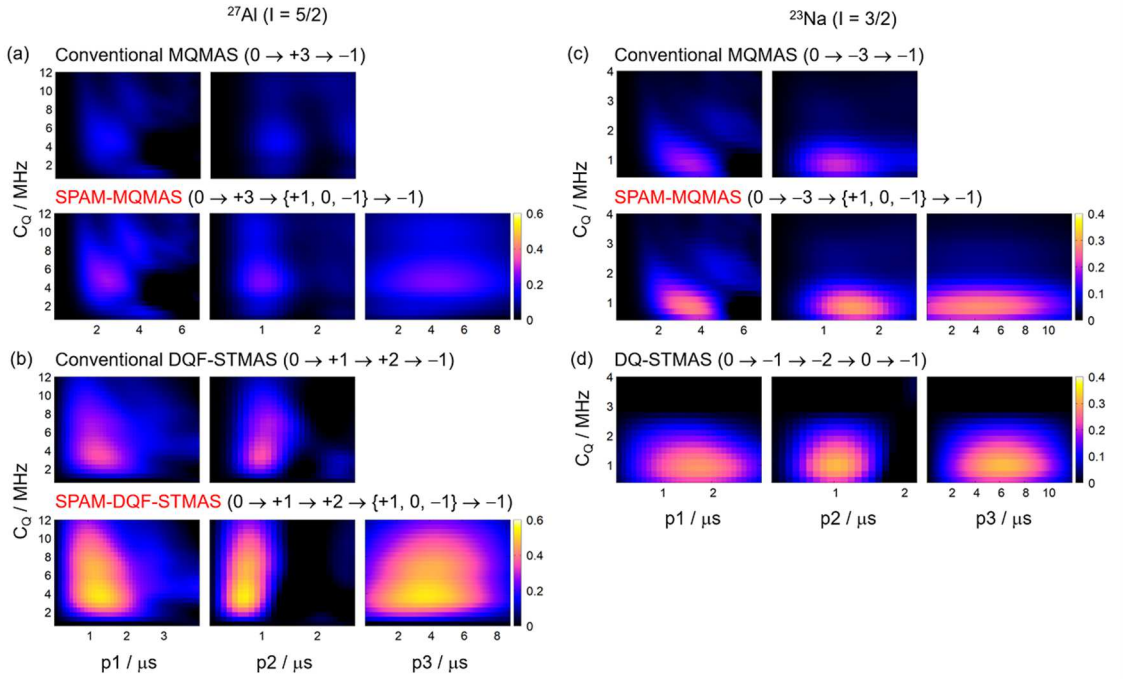

Fig.5. [IN COLOR] Simulated signal intensity for (a,b) ^{27}Al MQMAS and STMAS and (c,d) ^{23}Na MQMAS and DQ-STMAS with respect to each pulse length (p1, p2 and p3) for a range of C_Q values at B_0 = 14.1 T at ν_R = 62.5 kHz with ν_1 {p1, p2, p3} = {150, 150, 20} kHz. For each plot, one of the pulse lengths (denoted in the x-axis) is varied while others are fixed. Combination of pulse lengths used within each plot, {p1, p2 (Conventional/SPAM), p3}: (a) {3.0, 1.2/0.9, 4.0}, (b) {1.2, 0.9/0.7, 4.0} μs, (c) {3.5, 1.0/1.3, 6.0}, and (d) {1.4, 1.0, 6.0} μs.

recoupling time (τ_{dip}), the ^{1}H and ^{23}Na rf-strengths ($\nu_{1,H}$ and $\nu_{1,Na}$), and the read pulse length (P11). It should be noted that with $\{270_0,90_{180}\}$ basic element, the theoretically expected rf values are $\nu_{1,H}$ = 143 and 146 kHz for $PR16_7^6$ and $PR14_6^5$, respectively. The read pulse lasts 2 μs with $\nu_{1,H}$ = 125 kHz.

Similarly to RINEPT, (i) the CT-selective I pulses are very sensitive to the rf-field, whereas the ^{1}H recoupling and read pulses, both using large rf-fields, are robust with respect to their theoretical values, and (ii) the direct excitation of the ^{1}H magnetization by the recoupling pulses gives rise to undesired artefacts, which can be avoided with a ^{1}H pre-saturation pulse train. With $\{270_0,90_{180}\}$ basic element, the recoupling time may be estimated from the relation, $\tau_{dip} \approx 30/b_{HI}$,[36,37] but this value needs to be optimized experimentally.

For RINEPT and PRESTO, the possible artefacts due to the direct excitation of the ^{1}H magnetization by the recoupling pulses, must be avoided by applying a ^{1}H pre-saturation pulse train, although it slightly increases the experiment time. If technically possible, these pulses can be applied during the relaxation delay of the quadrupolar nucleus. In cases where CPMAS is found to give rise to any artefacts, then the ^{1}H saturation pulses should similarly be applied.

III.3. Setting up SPAM

Several sensitivity enhancement schemes have been successfully implemented in MQMAS (for MQ excitation and conversion between 1Q ↔ 3Q coherences via FAM,[42] DFS,[43] HS,[44] LP,[45] and Cos-LP[46]) and STMAS experiments (for 2Q ↔ 1Q conversion via FAM[47] and for ST excitation and conversion via LP[48]). Among other available schemes, SPAM is especially beneficial in that no complicated optimization process is required and hence it is easy to set up.[27–31] Recently, we have demonstrated that, in the context of MQ-HETCOR experiments, the signal loss due to the decreased 1Q ↔ 3Q transfer efficiency occurring under fast MAS may be easily compensated by the SPAM gain.[26] Upon SPAM, the conversion hard-pulse is replaced with a composite one, where the hard-pulse is immediately followed by a CT-selective π/2-pulse with a proper phase that depends on the desired coherence pathway. For the coherence pathway, with Δp = ±2 or ±4 for p2 (Figs.**1** and **2**), the SPAM phase condition is $\phi_3 = -\phi_2$ or $+\phi_2$, for I = 3/2 or 5/2, respectively. Compared to other schemes, no complicated optimization is required with SPAM and hence this composite pulse is easy to set up. In this study, the SPAM enhancement is incorporated in I = 3/2 MQ-HETCOR and I = 5/2 MQ/ST-HETCOR experiments. Since we have described the SPAM setup protocol for MQ-HETCOR experiments in our previous study, here we illustrate the equivalent set up mainly for ST-HETCOR experiments.

It should be remembered that the SPAM enhancement is only applied to the MQ/ST conversion, meaning that the MQ/ST excitation part remains unchanged, irrespective of the presence/absence of the SPAM pulse. This is illustrated in Fig.**5** which shows the simulated signal intensity of ^{27}Al and ^{23}Na MQ/ST excitation and conversion parts of our HETCOR sequences, with respect to each pulse length (p1, p2 and p3) for a range of C_Q values at B_0 = 14.1 T with ν_R = 62.5 kHz. These results can be extrapolated for our {^{27}Al}-^{1}H and {^{23}Na}-^{1}H spin pairs, respectively. While the initial excitation pulse length (p1) remains the same, the optimum conversion pulse length (p2)

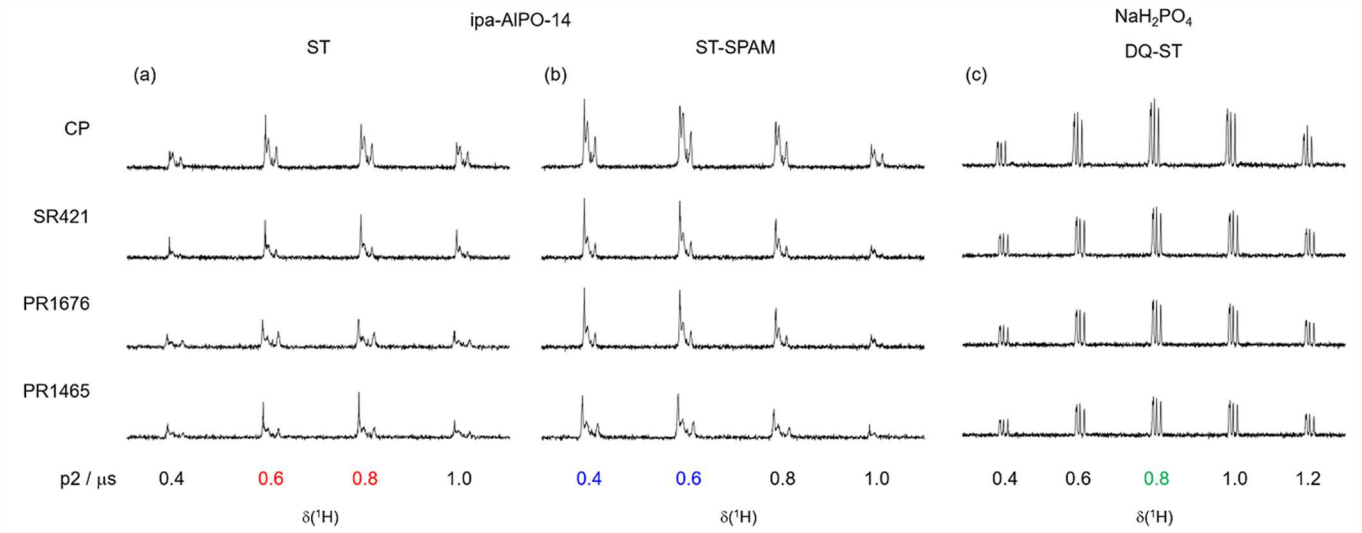

Fig.6. Examples of {^{27}Al}-^{1}H (a) ST-HETCOR, (b) ST-SPAM-HETCOR and (c) {^{23}Na}-^{1}H DQ-ST-HETCOR 1D profiles versus the p2 pulse length at ν_R = 62.5 kHz. (a,b) NS = 48, RD = 1 s, τ_{presat} = 300 ms, T_{exp} = 48-63 s each. (c) NS = 16, RD = 1 s, τ_{presat} = 500 ms, T_{exp} = 16-24 s each.

slightly changes upon SPAM, due to the difference in the selected coherence pathways. In our previous MQ-HETCOR study, we have experimentally confirmed that the optimum p2 pulse length is sensitive to a difference of a few tenths of µs, and this is similarly true for ST-HETCOR experiments. Fig.6 shows {^{27}Al}-^{1}H ST- and ST-SPAM-HETCOR, and {^{23}Na}-^{1}H DQ-ST-HETCOR 1D profiles versus the p2 length at ν_R = 62.5 kHz, using ipa-AlPO-14 and NaH_2PO_4, respectively. This length is varied by step of 0.2 µs, and its optimum value remains independent of the population transfer scheme that follows the MQ/ST conversion step. Our simulations are overall in good agreement with the experimental results. The conversion pulse length is the only crucial parameter upon acquisition of MQ/ST-HETCOR spectra with the SPAM enhancement.

IV. Comparison of MQ/ST-HETCOR 1D and 2D spectra

Using the optimum experimental conditions established in the previous sections, we compare the MQ/ST-HETCOR 1D and 2D spectra recorded with CP, RINEPT and PRESTO transfers. In the following, we call T_{exp} the experimental time, N_{t1} the number of t_1 increments, $t_{1,max}$ the maximum evolution time, Δt_1 the length of one t_1 increment, SW_{iso} the indirect isotropic spectral width,[33] NS the number of scans, RD the recycling delay, τ_{CP} the CPMAS contact time, and τ_{dip} the dipolar recoupling time of RINEPT or PRESTO (Figs.1 and 2).

IV.1. MQ/ST-HETCOR 1D spectra

Fig.7 shows the MQ/ST-HETCOR 1D spectra with CP, RINEPT and PRESTO transfers: either {^{23}Na}-^{1}H of NaH_2PO_4, Na_2HPO_4 and NaCD, or {^{27}Al}-^{1}H of ipa-AlPO-14. These 1D spectra correspond to the first FIDs (t_1 = 0) of the 2D

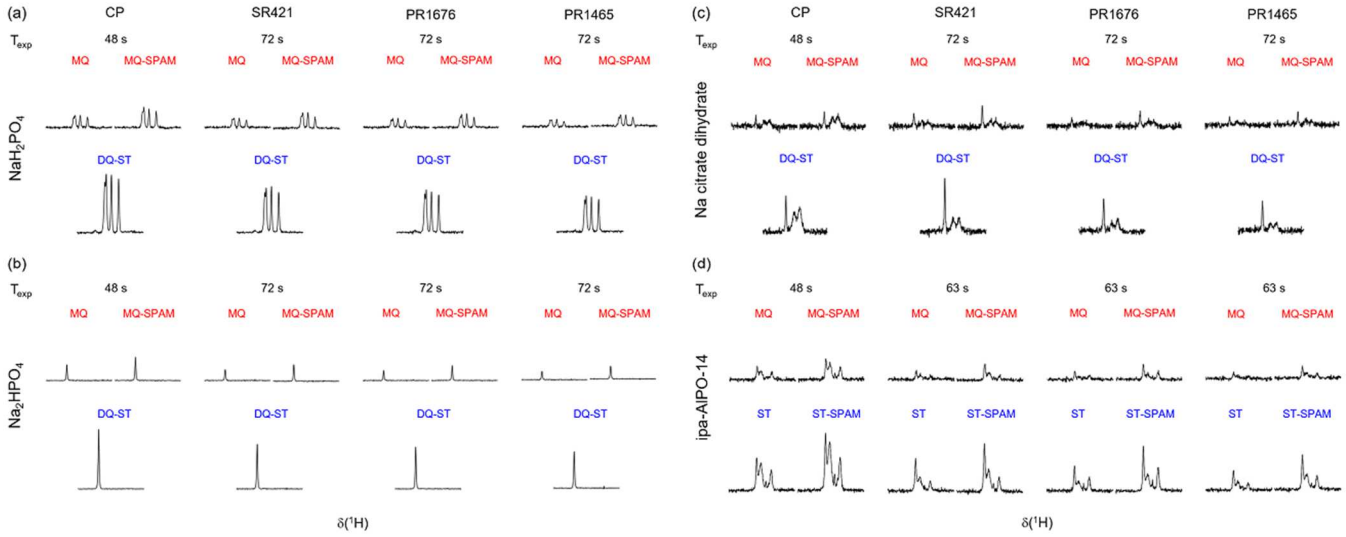

Fig.7. Comparison of (a-c) {^{23}Na}-^{1}H and (d) {^{27}Al}-^{1}H MQ/ST-HETCOR 1D spectra at ν_R = 62.5 kHz via CP, RINEPT and PRESTO transfers. (a) NaH_2PO_4, (b) Na_2HPO_4 (c) Na citrate dihydrate and (d) ipa-AlPO-14. NS = 48, RD = 1 s, τ_{presat} = 300-500 ms.

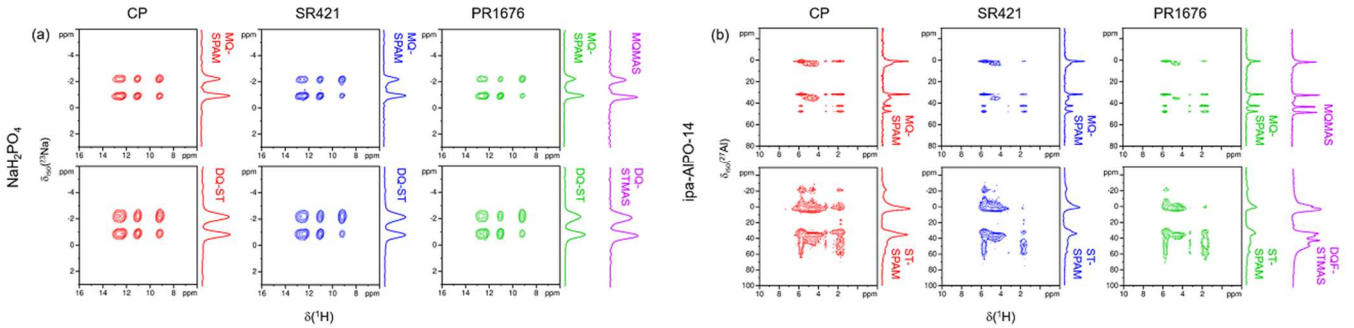

Fig.8. (a) {^{23}Na}-^{1}H and (b) {^{27}Al}-^{1}H MQ/ST-HETCOR 2D spectra of (a) NaH_2PO_4 and (b) ipa-AlPO-14 at ν_R = 62.5 kHz via CP, RINEPT and PRESTO transfers. An isotropic projection of the MQ/STMAS 2D spectra is shown on the right for comparison. NS {MQ, ST} = (a) {24, 16}, (b) {96, 96}. {RD (s), N_{t1}, $\Delta t_{1,MQ}/\Delta t_{1,ST}$ (µs), T_{exp} (h)} = {1, 300, 32/64, 1.3-3} and {0.5, 500, 16/16, 7-11}, for NaH_2PO_4 and ipa-AlPO-14, respectively.

acquisitions and their intensities are proportional to the integrated ones of the 2D spectra. The SPAM gain is expected to be 1.4 or 1.7, for I = 3/2 (^{23}Na) or 5/2 (^{27}Al), respectively,[19] and this is indeed observed experimentally. Upon comparison of the MQ/ST-HETCOR results, we find that the ST-HETCOR 1D signal is 2-4 times higher than the MQ-HETCOR counterpart. This is indeed consistent with the intensity differences that have been reported in the context of MQMAS and STMAS experiments.[31,35] Prior to the acquisition of 2D experiments that might last for a few hours or days, this quick 1D comparison of MQ/ST-HETCOR spectra serves as a preliminary guarantee of the sensitivity advantage of ST-HETCOR approaches.

IV.2. MQ/ST-HETCOR 2D spectra

Fig.**8** shows a series of {^{23}Na}-^{1}H and {^{27}Al}-^{1}H MQ/ST-HETCOR 2D spectra at ν_R = 62.5 kHz via CP, RINEPT and PRESTO transfers for NaH_2PO_4 and ipa-AlPO-14. The analogous 2D spectra for Na_2HPO_4, NaCD and Al-acet-lact are shown in Fig.**S2**. For NaCD and Al-acet-lact, only ST-HETCOR 2D experiments were performed, due to the low SNR of the MQ-HETCOR spectra. For PRESTO, we have only used $PR16_7^6$ for 2D acquisitions as it performed slightly better than $PR14_6^5$ upon 1D comparison (Fig.**7**). For the ease of comparison, Fig.**9** shows the corresponding isotropic projections of the series of 2D spectra of the five samples.

We observe that the differences in isotropic signal intensities between CP, RINEPT and PRESTO are comparable to those observed in 1D (Fig.**7**). When fully optimized for the best sensitivity, the three transfers yield similar 2D spectra, providing an identical information about the {I}-^{1}H spin system. Thus, these spectra should serve as a good starting point for

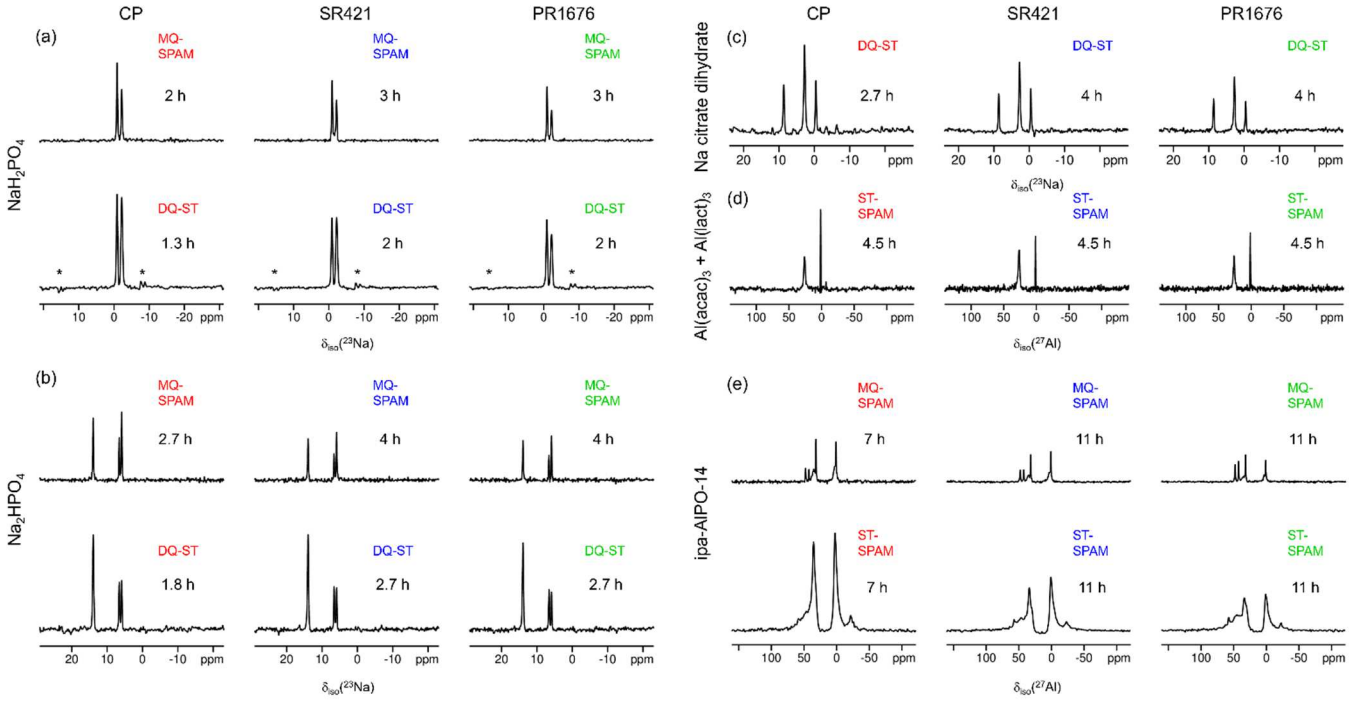

Fig.9. Comparison of isotropic projections of (a-c) {^{23}Na}-^{1}H and (d,e) {^{27}Al}-^{1}H MQ/ST-HETCOR 2D spectra at ν_R = 62.5 kHz via CP, RINEPT and PRESTO transfers. (The experimental details are given in the Fig.**8** and **S2** captions.)

more sophisticated experiments (e.g. distance measurements). Nevertheless, it can be observed that CP transfers are often slightly more efficient than the RINEPT and PRESTO ones. However, it must be reminded (i) that setting the CP transfers is more time-consuming than the RINEPT and PRESTO ones, especially in the case of ultra-fast MAS and low SNR, and (ii) that, contrary to CP and PRESTO, RINEPT transfers are not dipolar truncated, which means that they can more easily perform long distance transfers. Therefore, RINEPT transfers can be considered as a complementary tool to CP and PRESTO transfers.

In the ^{27}Al MAS 1D spectra of our 'artificial' mixture of aluminum acetylacetonate and lactate (Fig.**3**), we mentioned the presence of two C-H resonances that are resolved at ν_R = 62.5 kHz. In the corresponding {^{27}Al}-^{1}H ST-HETCOR 2D spectra (Fig.**S2c**), the ^{1}H resonances (OH, CH and CH_3) are clearly resolved and unambiguously assigned to the two Al samples via ^{27}Al-^{1}H correlations. As expected from the chemical structures, the OH is only present in lactate, whereas the CH and CH_3 species exist in both samples, with one CH peak at 5 ppm belonging to acetylacetonate, and that at 4 ppm to lactate.

It has been known that contrary to MQMAS, STMAS spectra are sensitive to dynamics in the µs time scale, leading to motional broadening in the isotropic dimension.[49] This is similarly true for ST-HETCOR experiments and here we demonstrate it using ipa-AlPO-14 (Figs.**8b** and **9e**). Indeed, the isotropic MQ-HETCOR peaks are narrow and well resolved as observed in the corresponding MQMAS, while the ST-HETCOR resonances are severely broadened. The isotropic ST-HETCOR line-shapes slightly differ from the corresponding STMAS ones, as shown with the vertical spectra in the last line in Fig.**8b**. This is because the ST-HETCOR scheme filters the ^{27}Al nuclei that are close to protons. These ipa-AlPO-14 spectra demonstrate that MQ/ST-HETCOR experiments are complementary approaches, like the MQ/STMAS pair, and that ST-HETCOR has the potential for further spectral editing in the presence of µs dynamics.

In I = 3/2 DQ-ST-HETCOR spectra, we notice the presence of additional small signals that are absent in the MQ-HETCOR ones. These are most apparent in the isotropic ST-HETCOR spectra of NaH_2PO_4 (Fig.**9a**), as denoted with asterisks. These sidebands, separated by $\nu_R/9$ = 6944 Hz, are consistent with the signal modulation due to the CT-selective π-pulse used for the 2Q filter being rotor synchronized only every 9 points. These additional peaks are also present, but smaller, in the isotropic ST-HETCOR spectra of Na_2HPO_4 and NaCD (Figs.**9b** and **9c**), making the DQ-ST-HETCOR spectra of I = 3/2 more 'crowded' than the MQ-HETCOR ones. We note that the position of these small additional peaks depends on the carrier frequency (Fig.**S3**).

Upon comparison of these MQ/ST-HETCOR 2D spectra, we emphasize that only a small part of the full 2D spectra is displayed in Figs.**8** and **S2**; that corresponding to the signal region**.** This leads to two practical important points to remind upon acquisition of MQ/ST-HETCOR 2D spectra. (i) The isotropic spectral width (SW_{iso}) is proportional to ν_R, and hence is very large under fast MAS, meaning that the signals are often concentrated on very small regions of the 2D spectra. (ii) For conventional rotor-synchronized experiments with $\Delta t_1 = T_R$, the SW_{iso} values are twice larger with STMAS than with MQMAS.[33] This means that, to keep the same isotropic resolution, twice more t_1 points must be acquired with ST-based experiments.

In the following section, we revisit and utilize these features to reduce the total experiment time of MQ/ST-HETCOR spectra shown in Figs.**8** and **S2**.

V. Reduction of the experiment time

The acquisition of MQ/ST-HETCOR 2D spectra under fast MAS often lasts for a few hours or days. This is mainly due to (i) the small sample volume in the small rotor and (ii) the large number of t_1 increments, due to the short rotor period, required to achieve an acceptable resolution in the indirect dimension.

To accelerate the acquisition of such time-consuming 2D spectra, we incorporate two 'tricks': an Optimized Rotor-Synchronization (ORS) and a Non-Uniform Sampling (NUS). Both tricks are applicable not only to MQ/ST-HETCOR, but also to MQ/STMAS experiments. In the following, we first demonstrate the practical advantage of the ORS using a series of MQ/ST-HETCOR 2D spectra under fast MAS. We then show several possible NUS schemes and discuss their potential in the context of high-resolution spectra of half-integer quadrupolar spin nuclei.

V.1. Optimized Rotor-Synchronization (ORS)

Usually, MQ/STMAS and MQ/ST-HETCOR experiments are performed in a conventional rotor-synchronized manner, with $\Delta t_1 = T_R$, making SW_{iso} proportional to ν_R. We have previously mentioned that our MQ/ST-HETCOR spectra are very 'sparse' under fast MAS because the signals are concentrated on a very small region of the 2D spectra (Figs.**8** and **S2**). This point can be utilized to decrease T_{exp} by only acquiring the FIDs every mT_R, $\Delta t_1 = mT_R$, which reduces SW_{iso} by the same factor m. This m value must be adjusted to the range of the resonances along the isotropic dimension. For example, at ν_R = 62.5 kHz, m = 1 means Δt_1 = 16 µs, whereas m = 2 means Δt_1 = 32 µs with a half SW_{iso} value, and so on. This is illustrated in Fig.**10a**, showing the reduction of SW_{iso} of the {^{23}Na}-^{1}H MQ/ST-HETCOR 2D spectra of NaH_2PO_4 at ν_R = 62.5 kHz.

In the following, we compare the results obtained with various ORS factors for two types of sequences: MQMAS vs. STMAS and MQ-HETCOR vs. ST-HETCOR. These various 2D acquisitions require very different T_{exp}. Therefore, to compare more easily the results for each sample, instead of the SNR, we use the **S**ensitivity of the isotropic projections defined as $S = SNR/\sqrt{T_{exp}}$.[7]

It must be noted that, upon reduction of SW_{iso} via the ORS folding factor, m, the thermal noise increases, as shown in Fig.**10c,d** where the corresponding isotropic projections of the 2D spectra are shown with their SNR and Sensitivities. The

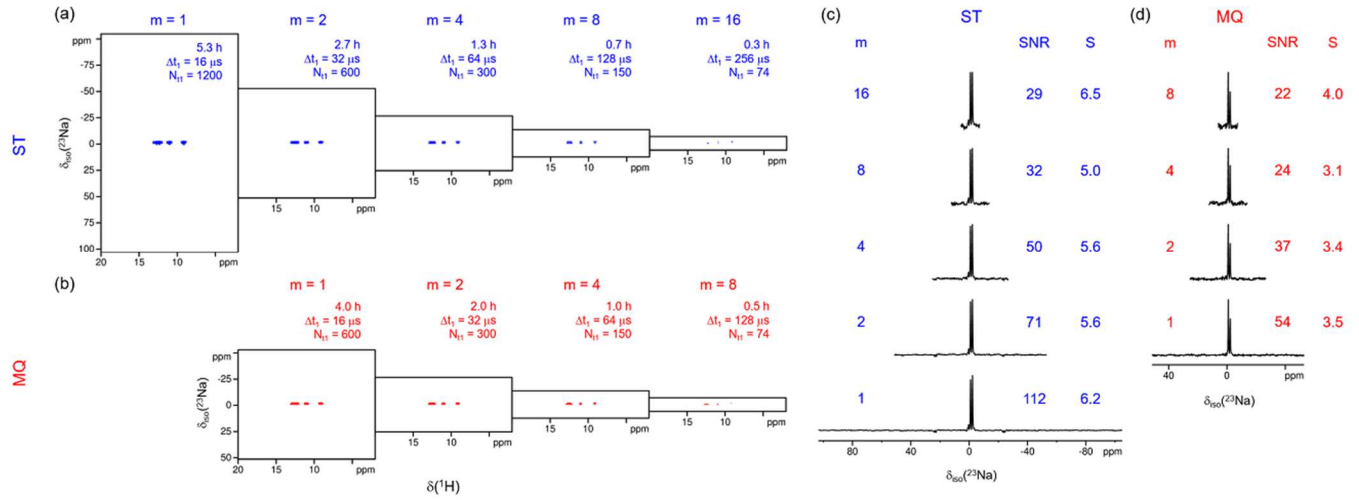

Fig.10. (a,b) Illustration of the reduction of SW_{iso} of MQ/ST-HETCOR 2D spectra using NaH_2PO_4 with {^{23}Na}-^{1}H CP transfer at ν_R = 62.5 kHz. (c,d) The corresponding isotropic projections with SNR at –0.9 ppm and Sensitivity: S = SNR/$\sqrt{T_{exp}}$. NS {MQ, ST} = {24, 16} and RD = 1 s.

difference in SNR for the spectra obtained with different m values is purely a signal averaging effect related to the number of scans acquired. Therefore, the SNR is roughly inversely proportional to $\sqrt{m}$, and hence the Sensitivity remains constant. As a result, ORS allows faster experiments, but does not change the Sensitivity. However, it must be noted that when the t_1-noise is comparable to or exceeding the thermal noise, then the use of a larger window may result in a better sensitivity because the t_1-noise can then be distributed over the larger indirect window.

To verify this point, we recorded at ν_R = 62.5 kHz a series of MQ/STMAS and MQ/ST-HETCOR spectra of the five samples with a variety of m folding factors. We used the same maximum $t_{1,max}$ evolution time to keep the same resolution, and m = {1, 2, 4, 8, 16}, which corresponds to Δt_1 = {16, 32, 64, 128, 256} μs, respectively. The corresponding SNR and Sensitivities are shown in Fig.**11**, and they show that Sensitivities are little dependent on the m factor.

As noted in the previous section, the ratio of SW_{iso} of the MQ- and ST-based 2D spectra is in the ratio of MQ:ST = 1:2, and ST-based experiments require twice more t_1 points than the MQ counterpart to obtain the same resolution along F_{iso}.

This means that, for a given spectrometer time, we can acquire a pair of MQ/ST-based spectra with the same SW_{iso} if we set the m value in the ratio of MQ:ST = 1:2. This was in fact utilized in the MQ/ST-HETCOR 2D spectra of NaH_2PO_4 and Na_2HPO_4 (Figs.**8a** and **S2a**) where m = 2 was used for MQ-HETCOR and m = 4 for ST-HETCOR. These experiments lasted twice or four times shorter than the m = 1 equivalent.

Although, the reduction of T_{exp} via ORS can be utilized in any 2D experiment, we note three practical cautions. (i) Since it decreases the SNR, that observed with m = 1 needs to be high enough. (ii) ORS is suitable for very sparse 2D spectra where the signals are concentrated in a small frequency range in the indirect dimension, which is quite often the case with high-resolution spectra of half-integer quadrupolar nuclei. (iii) ORS is especially powerful when a series of 2D experiments must be acquired within a given amount of spectrometer time but with different parameters or on different samples (as in Fig.**8**) for the purpose of spectral comparison.

V.2. Non-Uniform Sampling (NUS)

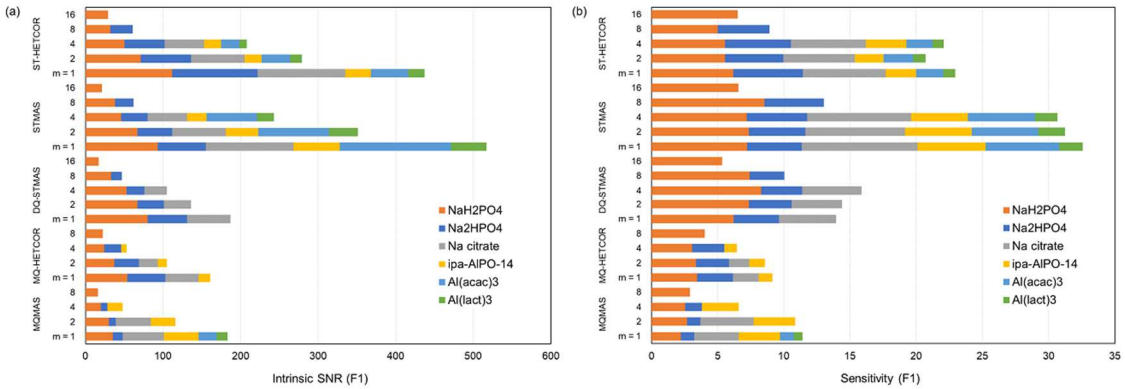

Fig.11. [IN COLOR] A summary of the intrinsic SNR (left) and Sensitivity (right) of a series of MQ/STMAS and MQ/ST-HETCOR spectra at ν_R = 62.5 kHz with respect to the reduction factor (m) in the isotropic spectral width (SW_{iso}).

The NUS acquisition has been used for a long time in solution NMR and MRI, and it has been particularly advantageous for multi-dimensional experiments, where only a limited number of points are sampled in the multiple indirect dimensions. In this case, the NUS allows a drastic reduction of the very long (or even practically inaccessibly long) experiment times.

In our high-resolution MQ/STMAS and MQ/ST-HETCOR 2D spectra, there is only one indirect dimension, where the isotropic signals are narrow because they are not quadrupolar-broadened with H_{Q1} and H_{Q2}. Thus, we expect that the same results obtained in solution NMR should apply.

There are two independent parts related to this type of acquisition: the NUS itself and the subsequent spectral reconstruction.

For solid-state NMR, there is a limited number of NUS studies using one reconstruction algorithm developed for solution NMR,[38] such as MaxEnt (maximum entropy),[50] SMILE (sparse multidimensional iterative lineshape-enhanced),[51] and CS (compressed sensing).[52] Here, we use the CS algorithm,[53] which has been proven to be superior to other methods when the spectrum is "mostly empty" (or sparse).[52] Also, for our convenience, we note that CS is available under the TopSpin free license. In the following, we test various NUS schemes in the context of 2D experiments with high-resolution quadrupolar resonances along the indirect dimension.

V.2.1 Basic concepts

First, we review some of the basic concepts that have been used in the context of NUS. In this study, we use the symbol T_2 for the exponential time constant of the transverse relaxation time, taking into account all experimental imperfections, such as the inhomogeneity of the static magnetic field.[43] The value of T_2 in the isotropic dimension of MQ/STMAS and MQ/ST-HETCOR spectra can be estimated in two ways: (a) in the time-domain, by fitting a series of 2D FIDs with an exponential decaying function, (b) in the frequency domain, by using the isotropic linewidth, $T_2 = 1/(\pi*\text{FWHM})$.

In conventional solution NMR with uniform sampling, it has been shown that to resolve two signals that are separated in the order of their linewidths, the maximum evolution time requires the condition $t_{1,max} \approx \pi T_2$, and that $t_{1,max}$ in the range of $(0.7\text{-}1.5)T_2$ has a negligible effect on the SNR of a given signal, although it reaches a maximum at $1.26T_2$.[54] This leads to the practical notions that (i) the resolution improves after $1.26T_2$ at the expense of both the SNR and T_{exp}, and (ii) upon uniform sampling of multi-dimensional experiments, one should choose the shortest evolution time that gives rise to the desired resolution.[55]

Contrary to the conventional uniform sampling, NUS is known to produce a Sensitivity gain without compromising the spectral resolution.[52,54] Two practical points should be kept in mind. (i) The NUS signal enhancement is only obtained with sufficiently long evolution times (i.e. $t_{1,max} \approx 3T_2$). This is because NUS uses an exponentially weighted sampling density in the indirect dimension such that the majority of sampling points are eliminated towards the end ($t_{1,max} > 1.26T_2$).[54] (ii) The estimation of the NUS gain requires the comparison between the conventional and NUS datasets acquired within the same overall T_{exp}. This means that the NUS dataset, which samples only X % points of the total Nyquist grid, contains 100/X-fold more scans.[52]

V.2.2 CS approach and possible sampling schemes

The CS (Compress Sensing) reconstruction approach has been recently investigated using ^{2}H MAS spectra, and it was suggested that the optimum CS approach should be obtained with an exponentially weighted decaying sampling with constant time: $T_S \approx 0.5\text{-}0.6T_2$.[52] Here, we extend this approach to the context of high-resolution spectra of half-integer spin quadrupolar nuclei. We apply the CS-IRLS algorithm to reconstruct the 2D spectra.[56] Indeed, compared to the analogous CS-IST algorithm, which is less memory consuming, faster in processing and hence more suitable for larger datasets, IRLS is known to provide better results with only slightly longer computational times.[53]

The NUS schemes can be characterized by (i) the percentage of sampling points with respect to the conventional full acquisition (e.g. 50%, 32% etc.), (ii) the nature of the sampling weighting (e.g. random or exponential), and (iii) the nature of the sampling spacing (e.g. random or increasing). In this present work, we compare four sampling schemes: the truly random, the exponential random with $T_s = T_2$ or $0.7T_2$, and a sampling with two exponential decays: one for the weighting and one for the spacing. The first three schemes, called NUS_{t1}, are available under the TopSpin free license, but the last one ($NUS_{bi\text{-}exp}$) is generated externally using a Python script (see the SI). These sampling schemes are schematically illustrated in Fig.**S4**. The two main differences between the NUS_{t1} and $NUS_{bi\text{-}exp}$ schemes are the nature of the sampling spacing and the $t_{1,max}$ value. The last sampled point is important because it determines the resolution of the indirect dimension and one would wish to use the same value as the conventional acquisition. For the NUS_{t1} scheme, we find this deviation more significant with a small NUS percentage (e.g. 32% in Fig.**S4b**,**d**) and a large Δt_1 values (e.g. 128 µs in Fig.**S4c**,**d**).

In the following, we test at ν_R = 62.5 kHz with the four sampling schemes the NUS effects in terms of signal reproducibility, with respect to the sampling percentage. We use a series of MQ/ST-based spectra of the five test samples, combined with the ORS described in the previous section.

V.2.3 Reproducibility of signals by the sampling schemes

As a preliminary result, we have previously shown a comparison of the isotropic projections of {^{27}Al}-^{1}H MQ-HETCOR spectra of ipa-AlPO-14 with a series of NUS sampling percentage (50, 33, 25 and 12.5%). We used the NUS_{t1} sampling scheme on TopSpin with T_s = 1 s (truly random), and we noted that down to ca. 30%, NUS may be safely employed in this case.[26] Here, we study the effects of the four sampling schemes in two ways. We perform first qualitative

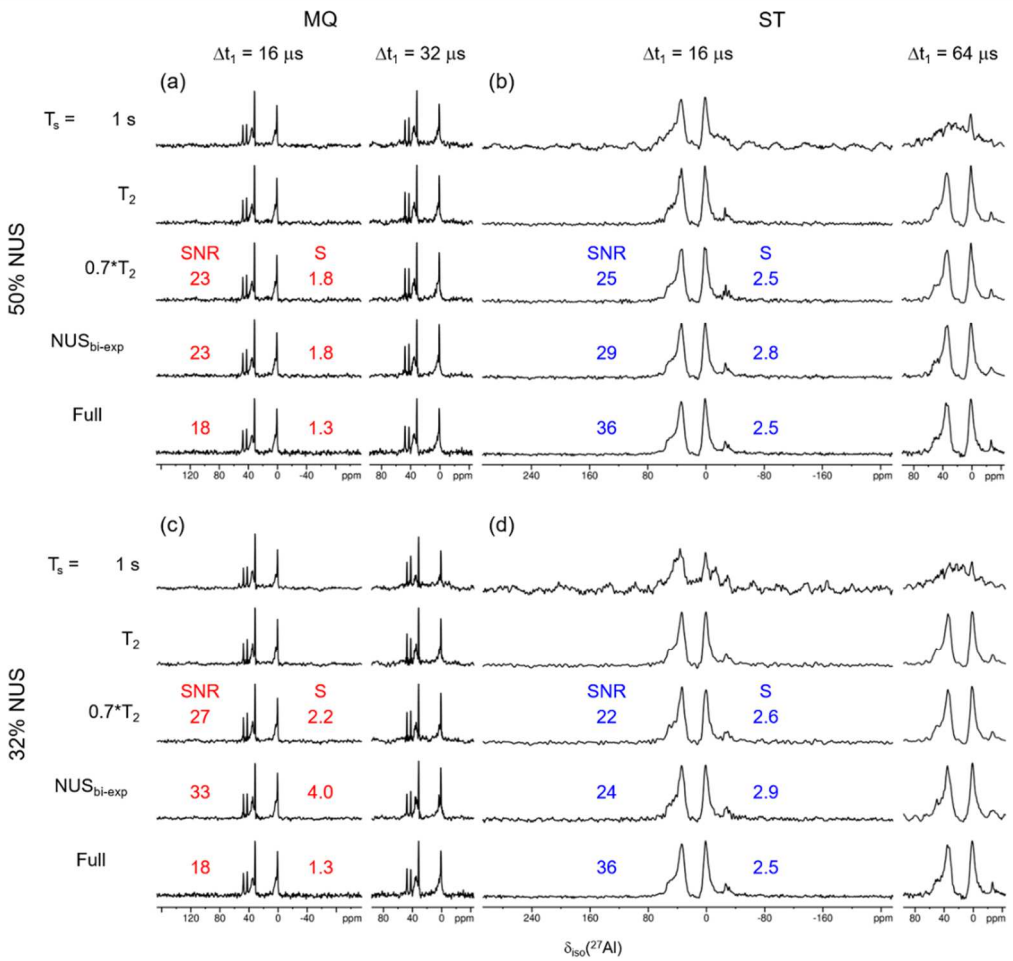

Fig.12. Isotropic projections of {^{27}Al}-^{1}H MQ/ST-HETCOR 2D spectra with CP transfers, with 50 (a,b) and 32 (c,d) % NUS with respect to the various sampling schemes, using ipa-AlPO-14 at ν_R = 62.5 kHz as an example. T_2 {MQ, ST} = {1.6, 0.25} ms. {Δt_1 (μs), Nt_1} = {16, 500} or {32, 250} (a,c) or {16, 500} or {64, 125} (b,d). The CS-IRLS processing (Mdd_mod = CS, Mdd_CsALG = IRLS) was performed on TopSpin with or without the Virtual Echo option (Mdd_CsVE = TRUE (MQ) or FALSE (ST)). For Δt_1 = 16 μs, the SNR and Sensitivities at δ_{iso} = 1 ppm of the Full (100 %) 2D spectra and of the two best ones acquired with NUS_{t1} ($T_S = 0.7T_2$) or $NUS_{bi\text{-}exp}$ are given.

comparisons of either the isotropic projections or the difference 2D spectra between conventional and NUS acquisitions. In a second step, we perform a quantitative analysis of the rms (root-mean square) of these difference 2D spectra integrated over the signal region.

Qualitative analyses. In Fig.**12**, as an example, we present the isotropic projections of {^{27}Al}-^{1}H MQ/ST-HETCOR 2D spectra of ipa-AlPO-14 at ν_R = 62.5 kHz, with either the full acquisition (100 %) or the 32 and 50 % NUS using the four sampling schemes. It should be reminded that, in the CS algorithm, the Virtual-Echo option (TopSpin: "Mdd_Cs VE = TRUE") provides better results when the phases in the indirect dimensions are known.[57] This is what we have verified with the MQ-HETCOR data. On the contrary, ST-HETCOR data provided better results without this Virtual-Echo option. This is because, in ST-based experiments, the first data point of the 2D FIDs (t_1 = 0) is missing due to the rotor-synchronization required to refocus the H_{Q1} broadening of ST coherences. This missing point leads to a large phase uncertainty in the indirect dimension, especially in the case of multiple sites.

The comparison of the isotropic projections in Fig.**12** proves a good reproducibility of the spectra, irrespective of the four sampling schemes we tested. To verify this observation in the entire 2D spectra, Fig.**13** shows, as an example, a series of difference (Full - NUS) 2D spectra with 50, 32, 24 and 12 % NUS using {^{27}Al}-^{1}H MQ-HETCOR of ipa-AlPO-14 at ν_R = 62.5 kHz with NUS_{t1} and $T_S = 0.7T_2$ = 1.1 ms.

These difference spectra demonstrate the lack of false peaks in the 2D spectra, but they also show that the amplitudes of the actual peaks are less well reproduced when the NUS sampling percentage decreases.

Quantitative analysis. We then performed a quantitative analysis by calculating the rms of the difference 2D spectra integrated over the signal region. These rms values are normalized with respect to the conventional 2D spectra over the same region. Fig.**14** summarizes the normalized rms differences of a series of MQ/STMAS and MQ/ST-HETCOR NUS 2D spectra at ν_R = 62.5 kHz with respect to the various sampling schemes for NaH_2PO_4 and ipa-AlPO-14. The analogous plots for the three other samples (Na_2HPO_4, NaCD,

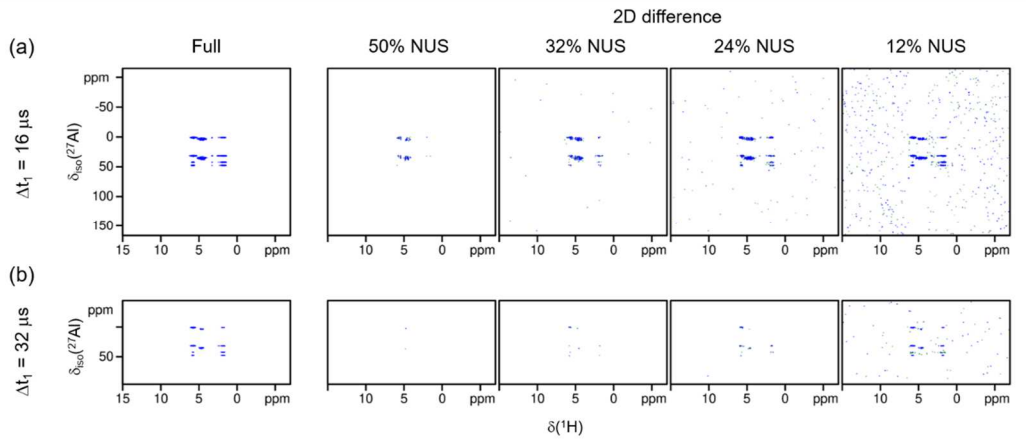

Fig.13. Examples of difference (Full – NUS) 2D spectra with 50, 32, 24 and 12% NUS, using $\{^{27}Al\}$-^{1}H MQ-HETCOR of ipa-AlPO-14 at ν_R = 62.5 kHz, with $T_s = 0.7T_2$ = 1.1 ms and (a) Δt_1 = 16 µs and (b) 32 µs, respectively. The full (i.e. non-NUS) 2D spectrum is also shown on the left for comparison.

Al-acet-lact) are provided in Fig.**S5**. As expected, when the NUS sampling percentage decreases, the differences increase. To minimize such signal errors in the NUS 2D spectra, we recommend two exponential decaying sampling schemes, either NUS_{t1} ($T_s = 0.7T_2$) or especially $NUS_{bi\text{-}exp}$.

V.2.4 Optimized rotor-synchronization combined with NUS

As a natural consequence, the NUS approach can be combined with the reduction of SW_{iso} via ORS (section V.1).

As an example, revising the $\{^{27}Al\}$-^{1}H MQ/ST-HETCOR spectra of ipa-AlPO-14, we have shown in Fig.**12** the isotropic 1D projections for Δt_1 (MQ, ST) = {16, 32} and {16, 64} µs, and in Fig.**13** the difference 2D spectra for Δt_1 (MQ) = {16, 32} µs. For completeness, the normalized integrated difference of a series of MQ/STMAS and MQ/ST-HETCOR NUS 2D spectra was summarized in Figs.**14** and **S5** with respect to the reduction factor of SW_{iso}.

Upon reduction of SW_{iso}, the global tendency remains the same: the difference increases as the NUS percentage decreases, but two appropriate sampling schemes, NUS_{t1} ($T_s = 0.7T_2$) and especially $NUS_{bi\text{-}exp}$, minimize such errors. However, we have observed that NUS with m > 4 brings no advantage because T_{exp} is already very short with m = 4, and the minimum safe limit of NUS then seems to be ca. 30-50% to limit the error. The latter point is partly due to the severely decreased SNR, proportional to $1/\sqrt{m}$, upon reduction of SW_{iso} (Fig.**11**).

So far, we have recommended the use of either NUS_{t1} ($T_s = 0.7T_2$) or $NUS_{bi\text{-}exp}$. Here, we revisit the last sampled point with these two schemes (Fig.**S4**), because this $t_{1,max}$ value determines the resolution of the indirect dimension. We note that with NUS_{t1} ($T_s = 0.7T_2$), $t_{1,max}$ decreases with a smaller NUS percentage and a larger Δt_1 value. This is reflected in the rms of the difference 2D spectra (Figs.**14** and **S4**), and NUS_{t1} thus may introduce an extra error due to the signal truncation. On the contrary, $NUS_{bi\text{-}exp}$ always leads to the same $t_{1,max}$ value, which is decided by the user, and thus, our bi-exponential sampling scheme may be superior in these cases.

V.3 Sensitivity gain per unit time via ORS and/or NUS

Our primary motivation to employ NUS and/or ORS in high-resolution quadrupolar experiments was to reduce the total experiment time of such long 2D acquisitions. However, we may perhaps utilize these two tricks to improve the quality of the 2D spectra by increasing the experimental Sensitivity ($S = SNR/\sqrt{T_{exp}}$).[7] It is indeed very important to remind here that when comparing different data acquisition and treatment, the only parameter to take into account is the Sensitivity, not the SNR, because T_{exp} may largely vary. When comparing different types of experiments, e.g. MQMAS vs. STMAS or MQ-HETCOR vs. ST-HETCOR, this comparison of the Sensitivity must be done with the same indirect spectral width, SW_{iso} here with the unified representation.[33]

When using NUS within the safe reduction limit, the Sensitivity largely increases when the sampling decreases, especially with $NUS_{bi\text{-}exp}$. As example, S increases from 1.3 to 4.0 when the sampling decreases from 100 to 32 % (Fig.**12c**). However, it must be noted that this gain mostly occurs because the resonances along F_{iso} are then narrow, and that it is more limited in the case of broad resonances (Fig.**12b**,**d**). This means that NUS is particularly interesting in the case of well-crystallized samples observed either with MQMAS or with STMAS (in the absence of µs dynamics).

For ORS, we have seen in Fig.**10c**,**d** that there is no Sensitivity gain. Therefore, ORS is mostly interesting in the case of sensitive experiments (large SNR with m = 1), to optimize and acquire fast the 2D spectra.

V.4 Miscellaneous discussions

We finish our article by answering some miscellaneous questions that may arise from a practical point of view, upon choosing: SW_{iso}, the NUS percentage, and the magnetization transfer scheme, in the context of MQ/ST-based high-resolution experiments of half-integer quadrupolar spin nuclei. The choice of SW_{iso} is related to the high spinning frequency

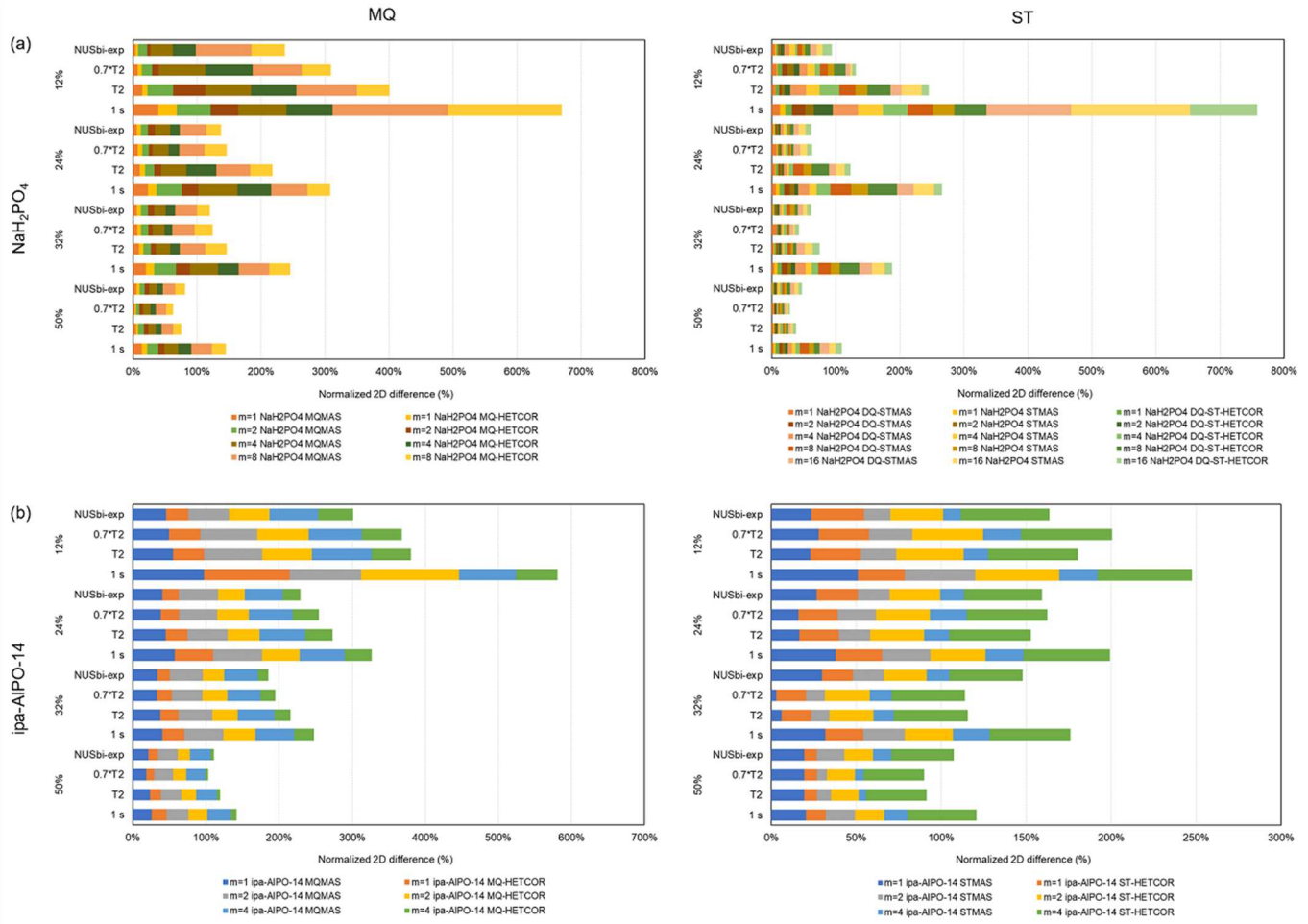

Fig.14. [IN COLOR] Normalized 2D integrated difference of a series of MQ/STMAS and MQ/ST-HETCOR NUS 2D spectra at ν_R = 62.5 kHz with respect to the various sampling schemes and the reduction of SW_{iso}. (a) NaH_2PO_4 and (b) ipa-AlPO-14. Note: m = {1, 2, 4, 8, 16} corresponds to Δt_1 = {16, 32, 64, 128, 256} µs.

used, which may entail a large value that can be deliberately reduced with ORS. The answers to these questions are related to the type of experiment that may be preferred for a given T_{exp}. As a global answer, this choice mostly depends on the SNR of the 2D spectra for the given sample.

MQMAS with m = 1 or STMAS with m = 2?

For a given type of experiment, (i) due to the aliasing of the t_1-noise into the smaller spectral width, the SNR with m = 2 is smaller by ca. $\sqrt{2}$ with respect to that with m = 1, but (ii) T_{exp} is decreased by a factor of 2, hence globally leading to a quasi-constant Sensitivity (Fig.10c,d). Simultaneously, the STMAS 1D signal is often larger by a factor of 2-4 than that of MQMAS (Fig.5). As said before, the experimental comparison between 2D experiments must be performed based on the Sensitivity with same SW_{iso}. In our case, this means between MQMAS (m = 1) and STMAS (m = 2) due to the doubling of SW_{iso} with STMAS. In Fig.10c,d, we observe a Sensitivity gain of ca. 1.6 for STMAS. Therefore, if the technical requirements can be satisfied, STMAS may be preferred, especially for large C_Q values and under fast MAS conditions, where the MQMAS efficiency is significantly reduced.[32] However, it should be remembered that ST-based experiments are sensitive to µs dynamics and hence the acquisition of both MQ/ST-based spectra may be advantageous in some cases (as demonstrated using ipa-AlPO-14 in Fig.8b).

MQ-HETCOR with m = 1 or ST-HETCOR with m = 2?

For I ≥ 5/2, the same logic as the previous question may apply. However, we should remember that DQ-ST-HETCOR may introduce some small additional sidebands for I = 3/2, leading to undesirable spectral crowding in some cases (as shown using NaH_2PO_4, Na_2HPO_4 and Na-CD in Fig.9a-c).

m = 1 with 25% NUS or m = 2 with 50% NUS?

Undeniably, this question remains controversial. We have demonstrated that NUS may increase the Sensitivity, whereas ORS does not. In general, we observe that NUS performs better when the SNR is high, which corresponds to narrow resonances as shown in Fig.12. Naively speaking, NUS seems to have difficulty differentiating the true signal from the noise when the SNR is small. Thus, the more sensitive one (i.e. m = 1) may be preferred. However, we also observe that the safe limit of the NUS percentage lies in between 25-50 % for our

samples, and below this safe limit, a peak splitting may appear, lowering the reproducibility of the 2D spectra. The origin of this peak splitting needs to be further investigated, probably from a more theoretical point of view. Presently, we suggest, for example, 32% NUS with m = 2 from the practical point of view, as a compromise for now.

Which magnetization transfer?

For the five model samples used in this study, the CPMAS transfers of magnetization from a half-integer quadrupolar spin nucleus to ^{1}H are slightly more efficient than the RINEPT and PRESTO ones (Fig.9). However, CPMAS requires much more parameters to optimize than the second transfers (only τ_{dip}). This means that the CPMAS optimization is much more time consuming, especially at ultra-fast MAS and with poor SNR. At ultra-fast MAS ($\nu_R \geq 60$ kHz), we hence recommend PRESTO-$\mathrm{PR16}_7^6$ {270_0,90_{180}} and especially RINEPT-$\mathrm{SR4}_1^2$ {180}. It must also be reminded that these two transfers are complementary tools, because the first is dipolar truncated whereas the second is not, which means that RINEPT can more easily perform long distance transfers than PRESTO.

VI. Conclusions

In this study, we have presented a comparison of MQ/ST-HETCOR spectra between half-integer spin quadrupolar nuclei (I = ^{23}Na or ^{27}Al) and ^{1}H, under fast MAS conditions. In a similar manner to our previous study, the SPAM method was utilized for the sensitivity enhancement, owing to its ease in experimental setup, and a step-by-step experimental setup procedure was established for PRESTO with the aid of simulations and a series of 1D acquisitions prior to such long 2D acquisitions. In accordance with what has been known in the context of MQ/STMAS experiments, we observed, upon comparison on MQ/ST-HETCOR spectra, that (i) the sensitivity advantage of ST-HETCOR over MQ-HETCOR is apparent as expected, and (ii) ST-HETCOR is sensitive to the presence of μs dynamics, and hence a comparison of MQ/ST-HETCOR 2D spectra similarly serves as a probe for the possible presence of the μs dynamics around the half-integer quadrupolar nuclei.

We have also compared three types of magnetization transfers at ultra-fast MAS from half-integer quadrupolar nuclei to ^{1}H: CPMAS, PRESTO and RINEPT.

We should emphasize that, in this study, we only have employed five selected model compounds to establish and demonstrate the experimental setup of ^{1}H-detected MQ/ST-HETCOR experiments under fast MAS conditions. For these crystalline compounds with small to moderate C_Q values, the CPMAS efficiency was found comparable to those of RINEPT or PRESTO. With larger C_Q values, we envisage that RINEPT or PRESTO methods may perform superior to CPMAS, especially under fast MAS conditions. These two transfers are moreover complementary: RINEPT can easily transfer over long distances, whereas PRESTO cannot. If one wishes to perform MQ/ST-HETCOR experiments on more challenging samples, such as (i) sites with larger C_Q values or small natural abundance, (ii) disordered materials, or (iii) systems with a large range of C_Q or dipolar couplings, our present datasets and experimental setup protocol should serve as a good reference point to ease their experimental setup.

Furthermore, aiming to reduce the total experimental time of such long MQ/STMAS and MQ/ST-HETCOR 2D experiments, we have incorporated two experimental tricks: the Optimized Rotor-Synchronization (ORS) and the NUS.

The ORS does not change the Sensitivity ($S = SNR/\sqrt{T_{exp}}$). Therefore, it is mostly interesting in the case of sensitive experiments with large SNR, to optimize and acquire fast the 2D spectra.

We have then investigated the potential use of NUS, by studying the effects of several sampling schemes, in the context of MQ/ST-based 2D experiments. We have shown that it can largely increase the Sensitivity, within the safe limit of ca. 30-50% NUS. Moreover, the use of the bi-exponential sampling we have introduced may be highly recommended for peak reproducibility. However, NUS is mostly applicable to the narrow, isotropic peaks in our high-resolution MQ/ST-based spectra, and further investigations may be awaited for broader peaks (e.g. second-order broadened peaks in F1).

Since our discussions were based solely on spectral observations, we envisage that a more advanced theoretical treatment (with more sophisticated algorithms and/or different sampling schemes) may have the potential either (i) to reduce the safe limit of the NUS sampling percentage or (ii) to improve the spectral reproducibility below the current safe limit of the NUS sampling percentage. Such further NUS developments are currently under investigations and will be reported elsewhere.

Conflicts of interest

There are no conflicts to declare.

Acknowledgements

The authors would like to thank Drs. Hideaki Kimura (Bruker Japan) and Sebastian Wegner (Bruker BioSpin GmbH) for their help with the implementation of the pulse sequences on TopSpin software, and Dr. Wolfgang Bermel (Bruker BioSpin GmbH) for providing the AU programs.

References

1 A. Goldbourt, E. Vinogradov, G. Goobes and S. Vega, *J. Magn. Reson.*, 2004, **169**, 342–350.
2 C. Martineau, B. Bouchevreau, F. Taulelle, J. Trébosc, O. Lafon and J. Paul Amoureux, *Phys. Chem. Chem. Phys.*, 2012, **14**, 7112–7119.
3 B. Bouchevreau, C. Martineau, C. Mellot-Draznieks, A. Tuel, M. R. Suchomel, J. Trébosc, O. Lafon, J. P. Amoureux and F. Taulelle, *Chem. Mater.*, 2013, **25**, 2227–2242.
4 J. Trébosc, O. Lafon, B. Hu and J. P. Amoureux, *Chem. Phys. Lett.*, 2010, **496**, 201–207.
5 J. Wack, R. Siegel, T. Ahnfeldt, N. Stock, L. Mafra and J. Senker, *J.*

Phys. Chem. C, 2013, **117**, 19991–20001.
6 M. K. Pandey, H. Kato, Y. Ishii and Y. Nishiyama, *Phys. Chem. Chem. Phys.*, 2016, **18**, 6209–6216.
7 A. J. Rossini, M. P. Hanrahan and M. Thuo, *Phys. Chem. Chem. Phys.*, 2016, **18**, 25284–25295.
8 N. T. Duong and Y. Nishiyama, *Solid State Nucl. Magn. Reson.*, 2017, **84**, 83–88.
9 A. Venkatesh, M. P. Hanrahan and A. J. Rossini, *Solid State Nucl. Magn. Reson.*, 2017, **84**, 171–181.
10 A. Venkatesh, X. Luan, F. A. Perras, I. Hung, W. Huang and A. J. Rossini, *Phys. Chem. Chem. Phys.*, 2020, **22**, 20815–20828.
11 L. Frydman and J. S. Harwood, *J. Am. Chem. Soc.*, 1995, **117**, 5367–5368.
12 Z. Gan, *J. Am. Chem. Soc.*, 2000, **122**, 3242–3243.
13 C. M. Morais, V. Montouillout, M. Deschamps, D. Iuga, F. Fayon, F. A. A. Paz, J. Rocha, C. Fernandez and D. Massiot, *Magn. Reson. Chem.*, 2009, **47**, 942–947.
14 S. H. Wang, S. M. De Paul and L. M. Bull, *J. Magn. Reson.*, 1997, **125**, 364–368.
15 S. Steuernagel, *Solid State Nucl. Magn. Reson.*, 1998, **11**, 197–201.
16 M. Roux, C. Marichal, J. L. Paillaud, C. Fernandez, C. Baerlocher and J. M. Chézeau, *J. Phys. Chem. B*, 2001, **105**, 9083–9092.
17 L. Delevoye, C. Fernandez, C. M. Morais, J. P. Amoureux, V. Montouillout and J. Rocha, *Solid State Nucl. Magn. Reson.*, 2002, **22**, 501–512.
18 C. Fernandez, C. Morais, J. Rocha and M. Pruski, *Solid State Nucl. Magn. Reson.*, 2002, **21**, 61–70.
19 J. W. Wiench, G. Tricot, L. Delevoye, J. Trebosc, J. Frye, L. Montagne, J. P. Amoureux and M. Pruski, *Phys. Chem. Chem. Phys.*, 2006, **8**, 144–150.
20 R. Siegel, J. Rocha and L. Mafra, *Chem. Phys. Lett.*, 2009, **470**, 337–341.
21 J. W. Wiench and M. Pruski, *Solid State Nucl. Magn. Reson.*, 2004, **26**, 51–55.
22 J. P. Amoureux, J. Trebosc, J. Wiench and M. Pruski, *J. Magn. Reson.*, 2007, **184**, 1–14.
23 S. E. Ashbrook, M. Cutajar, C. J. Pickard, R. I. Walton and S. Wimperis, *Phys. Chem. Chem. Phys.*, 2008, **10**, 5754–5764.
24 M. Castro, V. R. Seymour, D. Carnevale, J. M. Griffin, S. E. Ashbrook, P. A. Wright, D. C. Apperley, J. E. Parker, S. P. Thompson, A. Fecant and N. Bats, *J. Phys. Chem. C*, 2010, **114**, 12698–12710.
25 B. Bouchevreau, C. Martineau, C. Mellot-Draznieks, A. Tuel, M. R. Suchomel, J. Trebosc, O. Lafon, J. P. Amoureux and F. Taulelle, *Chem. - A Eur. J.*, 2013, **19**, 5009–5013.
26 A. Sasaki, J. Trébosc and J.-P. Amoureux, *J. Magn. Reson.*, 2021, **329**, 107028.
27 Z. Gan and H. T. Kwak, *J. Magn. Reson.*, 2004, **168**, 346–351.
28 J. P. Amoureux, L. Delevoye, S. Steuernagel, Z. Gan, S. Ganapathy and L. Montagne, *J. Magn. Reson.*, 2005, **172**, 268–278.
29 J. P. Amoureux, L. Delevoye, G. Fink, F. Taulelle, A. Flambard and L. Montagne, *J. Magn. Reson.*, 2005, **175**, 285–299.
30 J. P. Amoureux, A. Flambard, L. Delevoye and L. Montagne, *Chem. Commun.*, 2005, 3472–3474.
31 A. Sasaki, Y. Tsutsumi and J. P. Amoureux, *Solid State Nucl. Magn. Reson.*, 2020, **108**, 101668.
32 J. P. Amoureux, M. Pruski, D. P. Lang and C. Fernandez, *J. Magn. Reson.*, 1998, **131**, 170–175.
33 J. P. Amoureux, C. Huguenard, F. Engelke and F. Taulelle, *Chem. Phys. Lett.*, 2002, **356**, 497–504.
34 C. Huguenard, F. Taulelle, B. Knott and Z. Gan, *J. Magn. Reson.*, 2002, **156**, 131–137.
35 S. E. Ashbrook and S. Wimperis, *Prog. Nucl. Magn. Reson. Spectrosc.*, 2004, **45**, 53–108.
36 H. T. Kwak and Z. Gan, *J. Magn. Reson.*, 2003, **164**, 369–372.
37 M. Bak, J. T. Rasmussen and N. C. Nielsen, *J. Magn. Reson.*, 2000, **147**, 296–330.
38 A. J. Vega, *Solid State Nucl. Magn. Reson.*, 1992, **1**, 17–32.
39 J. S. Gómez, A. G. M. Rankin, J. Trébosc, F. Pourpoint, Y. Tsutsumi, H. Nagashima, O. Lafon and J.-P. Amoureux, *Magn. Reson.*, 2021, **2**, 447–464.
40 R. Giovine, J. Trébosc, F. Pourpoint, O. Lafon and J. P. Amoureux, *J. Magn. Reson.*, 2019, **299**, 109–123.
41 X. Zhao, W. Hoffbauer, J. S. auf der Günne and M. H. Levitt, *Solid State Nucl. Magn. Reson.*, 2004, **26**, 57–64.
42 P. K. Madhu, A. Goldbourt, L. Frydman and S. Vega, *Chem. Phys. Lett.*, 1999, **307**, 41–47.
43 A. P. M. Kentgens and R. Verhagen, *Chem. Phys. Lett.*, 1999, **300**, 435–443.
44 R. Siegel, T. T. Nakashima and R. E. Wasylishen, *Chem. Phys. Lett.*, 2005, **403**, 353–358.
45 I. Hung and Z. Gan, *J. Magn. Reson.*, 2021, **324**, 106913.
46 I. Hung and Z. Gan, *J. Magn. Reson.*, 2021, **328**, 106994.
47 T. J. Ball and S. Wimperis, *J. Magn. Reson.*, 2007, **187**, 343–351.
48 I. Hung and Z. Gan, *Phys. Chem. Chem. Phys.*, 2020, **22**, 21119–21123.
49 S. E. Ashbrook, S. Antonijevic, A. J. Berry and S. Wimperis, *Chem. Phys. Lett.*, 2002, **364**, 634–642.
50 S. Paramasivam, C. L. Suiter, G. Hou, S. Sun, M. Palmer, C. Hoch, D. Rovnyak and T. Polenova, *J. Phys. Chem. B*, 2012, **116**, 7416–7427.
51 G. Porat and A. Goldbourt, *Isr. J. Chem.*, 2019, **59**, 1027–1038.
52 K. Kazimierczuk, O. Lafon and P. Lesot, *Analyst*, 2014, **139**, 2702–2713.
53 K. Kazimierczuk and V. Y. Orekhov, *Angew. Chem. Int. Ed.*, 2011, **50**, 5556–5559.
54 D. Rovnyak, M. Sarcone and Z. Jiang, *Magn. Reson. Chem.*, 2011, **49**, 483–491.
55 D. Rovnyak, *Concepts Magn. Reson. Part A*, 2019, **47A**, 1–10.
56 E. J. Candès, M. B. Wakin and S. P. Boyd, *J. Fourier Anal. Appl.*, 2008, **14**, 877–905.
57 M. Mayzel, K. Kazimierczuk and V. Y. U. Orekhov, *Chem. Commun.*, 2014, **50**, 8947–8950.

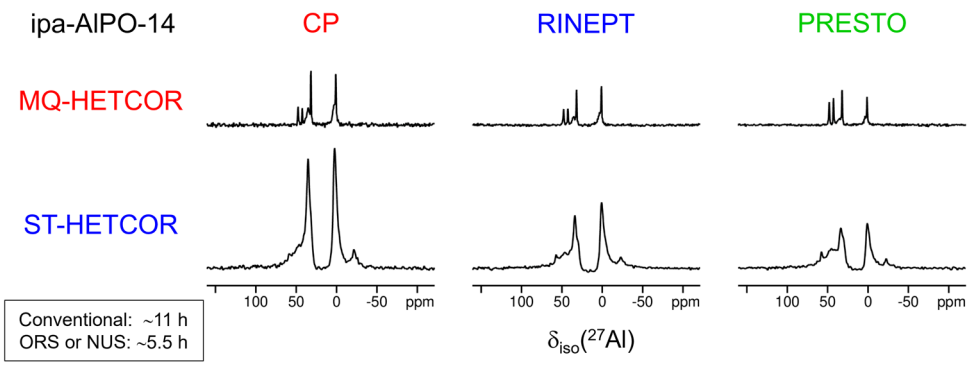

Isotropic projections of $\{^{27}Al\}$-^{1}H MQ/ST-HETCOR 2D spectra of ipa-AlPO-14 at ν_R = 62.5 kHz via population transfer by CP, RINEPT and PRESTO. The ST-HETCOR peaks are broadened due to µs dynamics.